HEALING SURFACE DEFECTS BY NANOCOMPOSITE COATING

Shang-Lin Gao, Edith Mäder, Rosemarie Plonka
Leibniz Institute of Polymer Research Dresden, Germany

Keywords*: nanocoatings; healing; surface flaw; nanotube; glass fibre*

Abstract

Surface defects of brittle materials cause real tensile strength much lower than the ultimate theoretical strength. Coatings can be used to 'heal' surface flaws and modify surface properties. Here, we describe an online process by which a nanometer-scale hybrid coating layer based on styrene-butadiene copolymer with single or muti-walled carbon nanotubes (SWCNTs, MWCNTs) and/or nanoclays, as mechanical enhancement and environmental barrier layer, is applied to alkali-resistant glass (ARG) and E-glass fibers. Our data indicates that the nanostructured and functionalised traditional glass fibers show significantly improved both mechanical properties and environmental corrosion resistance. With low fraction of nanotubes in sizing, the tensile and bending strength of healed glass fiber increases remarkably. No apparent strength variation appears for nanoclay coated fiber subjected to alkaline attack. We introduce a healing efficiency factor and conclude that the coating modulus, thickness and roughness are responsible for the mechanical improvement of fibers. Besides, nanocomposite coatings result in enhanced fiber/matrix interfacial adhesion, indicating nanotube related interfacial toughening mechanisms.

1 Introduction

Most solid materials have surface defects. For glass and other brittle materials, surface defects cause the measured mechanical properties significantly lower than their theoretical values. The nanoscale surface defects providing extra stress at the tip of the cracks can lead to stress-corrosion cracking at low stress level, particularly in a humid environment. Our recent work showed that the surface critical flaws have sizes in a range of a few hundred nanometres which encouraged us to investigate whether the nano-reinforcements with similar size functions as a crucial role for healing [1, 2]. Healing nanoscale surface flaws and enhancing materials' lifetime by nanocoatings, therefore, are important for many traditional materials.

Reinforcement with nanomaterials is a topic of significant current interest. It is well known that surface defect-free and high purity carbon nanotubes have exceptional high Young's modulus and tensile strength. However, an efficient utilization of the excellent properties of nanoreinforcements to the microscopic and macroscopic level is a long standing problem. To date, the highest strength and Young's modulus reported in the literature are relatively disappointing: 1.8~3.2 GPa and ~ 40 GPa, respectively, for aligned nanotube composite bundles with very high volume loading of nanotubes (60 wt%) [3, 4], which are a factor of ten below those of the component individual nanotubes because of poor integration and weak interfacial adhesion. Therefore, to find an appropriate dispersion for the nanoreinforcements to increase volume concentration, limited by chemical inertness and van der Waals attractions, is not sufficient for producing high-quality composites. In contrast to this 'super-materials degraded by defects' approach, here, we apply a 'surface defects healed by super-materials' approach (Fig. 1), where the traditional alkali-resistant glass fibers (ARG) were coated using different nanostructured coating layers with low loading (<1 wt%) of single and multi walled carbon nanotubes (SWCNTs, MWCNTs) and/or organoclay to provide a protective layer against aqueous alkaline solution. AFM, SEM, TEM and single fiber tensile, bending and pull-out tests were used to

investigate in detail the local surface topography, the mechanical and the interfacial properties.
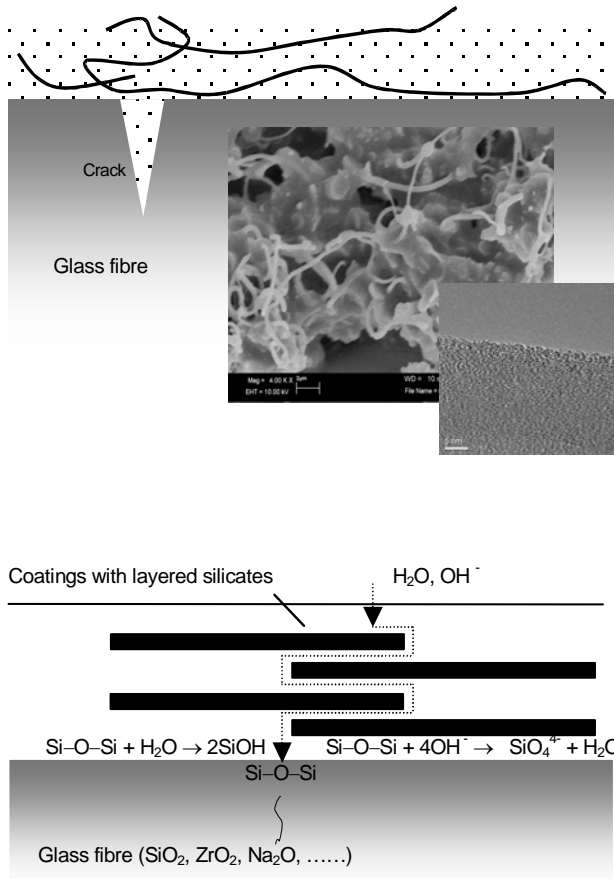
Crack

Glass fibre

Coatings with layered silicates H$_2$O, OH$^-$

Si–O–Si + H$_2$O → 2SiOH   Si–O–Si + 4OH$^-$ → SiO$_4^{4-}$ + H$_2$O

Si–O–Si

Glass fibre (SiO$_2$, ZrO$_2$, Na$_2$O, ……)

Fig. 1. Schematics of nanostructed coatings with MWCNTs or layered silicate network on glass fiber surface to enhance flaw healing effect and corrosion resistance. The inserts show polymer/ MWCNTs network by SEM and individual surface functionalized nanotube structure by TEM.

2 Experimental

2.1 Materials

The control ARG with diameter of 17 µm and E-glass fibers with diameter of 20~23 µm utilized in this work were made at our institute. Thermoplastic polypropylene filaments with diameters of 26 µm are produced from homopolymer PP (HD120M) and 2% Exxelor PO 1020 which acts as the compatibiliser. During the continuous spinning process, the ARG fibers were in-situ sized by an alkali-resistant sizing consisting of silane coupling

agent, γ-aminopropyl-triethoxysilane, in conjunction with film formers and nanoparticles in the aqueous sizing, namely S1. The 0.2 wt% surface functionalized MWCNTs (IFW, Germany) are dispersed in the epoxy film former based sizing. We applied surface coatings to the control ARG using either two kinds of styrene-butadiene copolymers with different T_g values (C1) or a commercial self-crosslinking styrene-butadiene copolymers (C2). Similarly, E-glass fibers were also coated with less than 0.5 wt% nanotubes in the coatings. The organo-clay particles (Nanofil 15, Süd-Chemie AG, Moosburg, Germany) in maleic anhydride grafted polypropylene with a size of about 60 to 130 nm are dispersed in the obtained solution. A quaternary ammonium surfactant and a non-ionic surface active agent were added to the dispersion for homogeneous distribution of the constituents with or without 1 wt% nanoclay. This method benefits from its ambient temperature treatment and environmentally friendly deposition, in addition to chemical versatility. The total weight gain due to the coatings is 5.3 wt% measured by pyrolysis (600 ^{o}C, 60 min) of the coated fibers. We extracted the fibers in selected highly concentrated aqueous alkaline solution (5 wt % NaOH, pH of 14) at 20 ^{o}C for seven days, which is the most aggressive and corrosive condition to the fiber surface.

2.2 Characterization

Atomic force microscopy (AFM): An AFM (a Digital Instruments D3100, USA) was used as a surface morphology imaging tool to detect fibers, coatings and fracture surfaces. The topography and phase images of samples were studied in tapping mode, while phase shifts, i.e., changes in the phase angle of vibration with respect to the phase angle of the freely oscillating cantilever, recorded simultaneously with height changes, are present as a phase image. The phase images reveal differences in surface properties of the material which are currently only qualitative in nature. The cantilever (ULTRASHARP NSC16/50, MikroMasch, Estonia) has a normal spring constant of 35 N/m, a tip cone angle of 20°, radius of 5~10 nm and modulus of 160 GPa to assure good imaging resolution. Specimens were prepared by fixing separate short fibers on a silicon wafer, within a thin layer of pre-coated epoxy at the bottom side of the fiber.

Single-fiber tensile and bending test: The tensile strength of single fiber was measured using the Fafegraph mechanical testing device (Fa. Textechno) equipped with a 10 N force cell. The

gauge length is 20 mm and the cross velocity is 10 mm/min under 65% relative humidity and 20 °C according to specification EN ISO 5079. Based on a vibration approach, the diameter of each selected fiber was calculated from the fineness value, which was measured with a Vibromat ME (Fa. Textechno) according to specification EN ISO 53812 and ASTM D 1577. To verify the effect of surface properties on the statistical distribution of fiber tensile strength, the cumulative fracture probability, F, was fitted by single Weibull distribution model through the least squares method and the Weibull modulus m_o was calculated.

Due to the small dimensions of glass fiber, the bending strength is measured by means of a loop test [5]. The fiber is made into a loop which was forced between two parallel glass plates with distance of ten times of fiber diameter; at the same time, the fiber is attached to the jaws of the a self-made tensile testing machine which is mounted on an optical microscope. By pulling both ends of the fiber, the radius of curvature of the loop, R, decreases and eventually the fiber breaks due to bending; the smallest radius of curvature a fiber will allow before breaking is recorded. For an isotropically elastic fiber with modulus of elasticity, E, and diameter, d, bent to a large radius of curvature (large with respect to fiber diameter), based on the simple bending theory under the assumption of linear elasticity, the failure bending moment, M, and maximum bending stress, σ_{max}, at outside of a curved fiber are

$$M = \frac{\pi d^4 E}{64R} \qquad (1)$$

$$\sigma_{max} = \frac{dE}{2R} \qquad (2)$$

Single-fiber pull-out test (SFPO): Using embedding apparatus enabling PC-controlled temperature and time cycles, the model microcomposites for the single fiber pull-out test were prepared by accurately embedding the single fibers in matrix with embedding lengths of 100 through 200 μm. The pull-out test was carried out on a self-made pull-out apparatus with force accuracy of 1 mN and displacement accuracy of 0.07 μm with identical pull-out velocities (0.01 μm/s) at ambient temperature. The local interfacial adhesion strength, τ_d, and the critical interphase energy release rate, G_{ic},

can be determined by using the algorithm described previously [6, 7].

3 Results and discussion

3.1 Nanocomposite coating morphology

We first examined the morphology of nanoreinforcements in coatings. Fig.2 shows a pair of AFM topography/phase images of a nanocoating with nanotubes from identical areas captured on the glass fiber surface. Although it is normally impossible to observe the individual nanotubes when they are embedded in thick coating polymer matrix, our phase image on the fiber surface where the coating layer is thin shows apparent contrast between the nanotubes and the polymer regions. It reveals a difference in surface or underlying material properties of the regions in terms of roughness, stiffness, viscosity, and adhesion. Interestingly, the nanotubes show an irregular distribution and quite well separated from bundles which do not tend to normally agglomerate and build closely-packed patterns, suggesting that the high speed on-line sizing process could be utilized for separation of nanotube bundles for a wide range of composite applications.
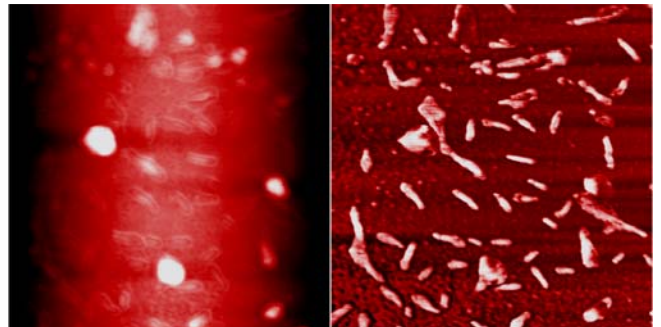

Fig. 2. AFM topography (left) and phase (right) images (x, y = 1 μm) of ARG with nanostructured coating with nanotubes.

We have further examined whether the dispersed organoclay was intercalated or exfoliated in the coatings. Individual crystallites observed by AFM topography (Fig. 3a) display the lath-type morphology of hectorite, consisting of a layered structure of aluminum sandwiched between two layers of silicon. The measured height of individual particles equals ~ 1.5 nm, which corresponds to the

distance between two single smectite layers. Fig. 3b shows that the fracture surface topography of coating film with clays after alkaline treatment consists of many similar shape particles. The measured thickness and lateral size of the particles are ~ 6 nm and ~ 80 nm, respectively, suggesting that the silicate layers of clay are intercalated. These clay platelets provide high surface areas of contact with the polymer matrix. Random distribution of the particles dispersed in the coating polymer matrix is clearly visible which are impermeable to molecular species and limit the diffusion of hydroxyl ions to glass surface and the crack tip. Obviously an appreciable level of platelet content and orientation is required to provide alkali barrier enhancement.
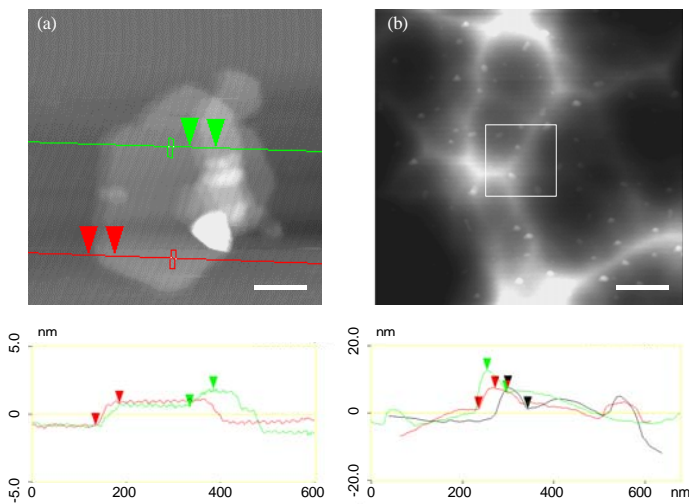

Fig. 3. AFM topography and section analysis (bottom) of (a) layered silicate clay and (b) fracture surface of coating with clay after alkali treatment. The distance between clay sheets is ~1.5 nm shown by section profile of the individual clay sheet along the lines in the top view of the left figure. Scale bars represent in (a) 100 nm and (b) 500 nm, respectively.

We have recently measured the sorption isotherms of fibers to understand the barrier levels that can be achieved with the nanometre-thin sheet-like layers of clay fillers in the coating [8]. The nanoclay containing coating has lower values of both adsorption and desorption than coating without clay at all ranges of relative pressure, suggesting that the clay coating adsorbs less water and the diffusion through the clay loaded coating appears much slower. Since a transport barrier layer affects both

diffusion and sorption, a proposed mechanism of the improving alkali-resistance is that the clay particles retain water molecules and reduce the moisture adsorption and concentration in the coating layer and coating/fiber interface. The clay particles also act as obstacles forcing both outside solution molecules and inside dissolved alkali ions diffusing to long detours around the platelets (cf. Fig.1). A number of experimental and theoretical studies of polymer film with clay have also shown that the intrinsic permeability decreases significantly, i.e., the water diffusivity was reduced to half of its value in the neat polymer [9,10]. Additionally, taking into consideration of chemical effects of coating, as revealed by Zetapotential measurements in our early work [11], the acidic groups (i.e. COOH) of coating polymer were dominating on fiber surface before and after NaOH treatment. Since the congruent dissolution of glass corrosion process is only valid in high pH environment, the coating with acidic character, as an alkali-deficient layer, can slow down the deterioration process by limiting the increase of the localized pH value and growth of silica gel layer. Therefore, the clay reinforced coating layer is rather alkali-resistant because of these different physico-chemical mechanisms.

3.2 Fiber tensile strength

We next investigated the tensile performance of the single fibers. Fig. 4a shows that the tensile strength of surface nanostructured ARG with both nanotubes and organoclay are significantly improved. The fiber strength increased up to 70 % and 25 % for sized fiber with 1 wt% loading of MWCNTs or organoclay in the sizing or coating, respectively. Because the critical flaws which limit the strength of fibers are located at the surface, the fiber fracture behaviour is strongly affected by the variation of coating properties. The varied breaking strength of glass fiber can be attributed to the distribution in flaw severity along the fiber length, where micro-cracks can be inherent to the glass itself or a result of the manufacturing process and handling of the fiber. Interestingly, as shown in Fig. 4b, both the Weibull plot lines and Weibull modulus, m_o, of coated systems shifts to higher values than those of the control. This indicates that the strength-controlling surface defects have lower heterogeneity distribution and the size of defects is reduced after healing. In other words, the healed flaws on the coated fibers show similar flaw size, severity and homogeneity compared to those on the control fibers.
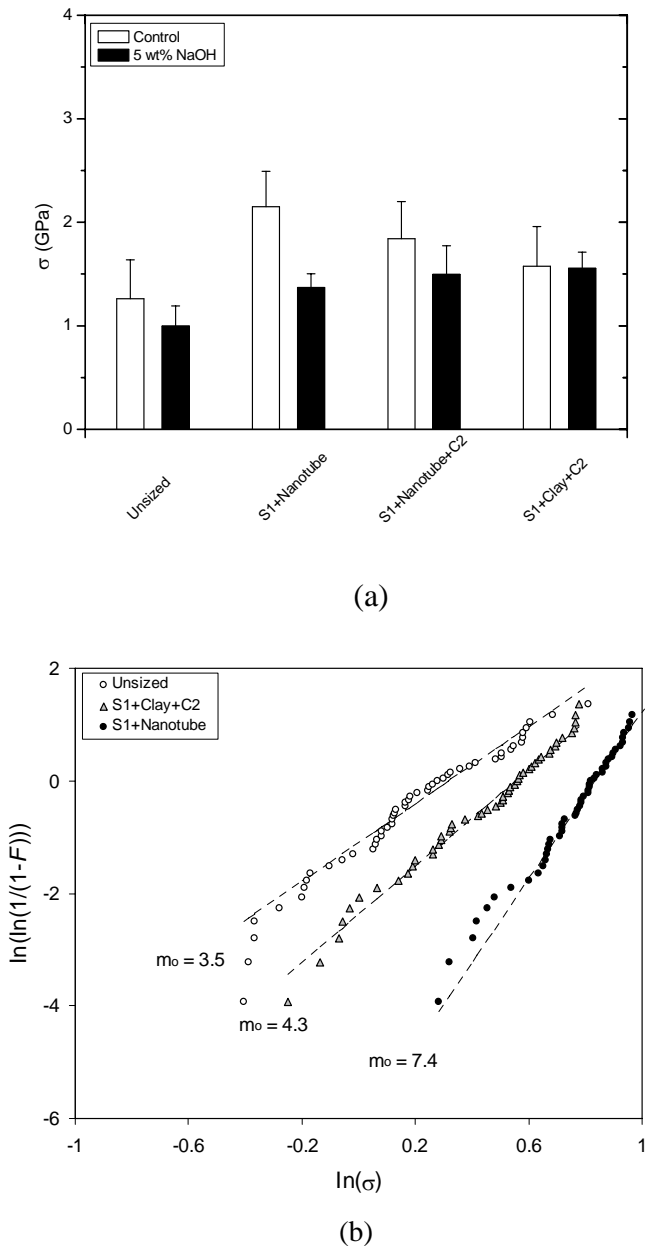
(a)

(b)

Fig. 4. (a) Effect of the nanostructed coatings with low fraction of nano-reinforcements on the tensile strength of ARG before and after alkaline treatment in 5 wt% NaOH aqueous solution for seven days in an ambient environment. (b) Weibull plots of fiber fracture probability. Error bars represent standard deviations for the estimate of the mean strength of fifty samples.

Additionally, the effects of alkaline attacks on the average fiber strength are also compared in Fig. 4a. It is evident that the sample of clay coatings would not yield a significant strength reduction upon alkali treatment. However, a significant strength

reduction for systems with nanotube sizings occurred. This can be partly compensated by an additional styrene-butadiene coating with carboxylic groups, which shows an enhanced alkali-resistance as determined by the marginal strength reduction. Therefore, the durability and alkali-resistance are also improved, particularly the fiber with organoclay coatings. Overall, the coated fibers have higher strength values than the control one after alkaline corrosion, reflecting the improved environmental durability for fibers with nanostructured coatings.

Potential mechanisms include the contributions of different factors for the mechanical property improvement by reducing the fiber surface flaw formation and crack growth. Note that the polymer coatings have Young's moduli that are typically several orders of magnitude lower than the glass fiber, and therefore do not bear a significant portion of the mechanical load. Although the polymer coatings do not increase strength, they have the important function of protecting the glass surface from abrasion and chemical damage, which in turn would degrade glass fiber strength. The coating layer with organosilicate plates could prevent moisture/alkali contact and reaction with glass lattice at a crack tip (stress corrosion). As aforementioned, the acidic groups of coating molecular interact with or absorb free cations and anions of environment leading to a slow-down of the corrosion process. Secondly, stress-redistribution and crack stopping mechanisms can be achieved by coatings and nanotube's 'bridging' effect and interface debonding/plastic deformation around crack tip. The mechanical 'healing' effect was viewed as a disappearance of the severe surface flaws because of an increase of the crack tip radius, the flaw filled by coatings being either elliptical than sharp. Thirdly, compressive stress on fiber surface might prevent crack opening/propagation by the shrinkage of polymer due to solidification. To simplify the complex phenomena, we developed a simple mechanical model based on Griffith fracture mechanics to roughly estimate the strength of coated fiber [8]. We consider a smoothly coated fiber loaded in tension and having a thin circumferential crack (Fig. 5). When the crack appears, the strain energy is released in a material volume adjacent to the crack. It is assumed that this volume is comprised by a conical ring whose generating lines are shown by broken lines and heights are proportional to the crack length. On the other hand, the energy is consumed by formation of new surfaces and deformation of coatings because of an

elastic constraint. According to the energy balance, the coated fiber strength, σ_f, can be expressed as

$$\sigma_f > \overline{\sigma}_f = \sqrt{\frac{2\gamma E_f}{(\beta a^* - \frac{L(1 + L/d)E_c}{E_f})}} \quad (3)$$

where γ is fracture surface energy and β is a constant coefficient of proportionality. E_f and E_c are Young's modulus of fiber and coatings, respectively. We used an apparent crack length a^* instead of a to take into account geometrical influences of surface defects arising from either coatings filling of crack tip or surface roughness. Notably, the critical tensile stress of fiber with a surface flaw, $\overline{\sigma}_f$, is significantly affected by the coating modulus and thickness. Accordingly, we propose a nondimensional healing efficiency factor, $\varphi = L(1+L/d)E_c/\beta a^* E_f$ as an indication of whether the fiber is sufficiently coated and how the reinforcement effect is degraded by environmental corrosion. Therefore, the strength improvement ratio, η, can be related to a healing efficiency factor, φ, as

$$\eta = \frac{\sigma_f - \sigma_o}{\sigma_o} = \frac{1}{\sqrt{1 - \varphi}} - 1 \quad (4)$$

where $\sigma_o = (2\gamma E_f/\beta a^*)^{1/2}$ is the strength of the fiber without coatings. More rigorous analysis shows that reducing a^* to equilibrium interatomic distance, a_o, of atoms at force equal to zero, σ_o approaches the ultimate theoretical strength of fiber, $\sigma_{max} = E_f/2\pi$. The healing efficiency factor ranges from zero to one representing conditions from non-coating/poor healing case until efficient healing. Overall, our glass fibers with nanotube coatings show the highest η and mechanical strength improvement (Fig. 6). Generally speaking, the thicker the coating layer and larger the stiffness of the coatings the higher is φ and tensile strength of the fiber. On the other hand, the larger the size of defect and higher the stiffness of fiber, for effective repairing, the thicker and stiffer coatings are required. It implies that the higher strength can be achieved for fiber with surface defects when the healing efficiency factor is more close to one. Moreover, the variation of healing efficiency factor indicates how strong the resistance of the coatings subjected to environmental attack, i.e., no significant reduction of φ for

nanoclay coatings after alkaline treatment represents its high environmental barrier and anti-corrosion property. Finally, the model allows to estimate approximately the coating stiffness based on the tensile strength of fibers. Taking as estimate $E_f = 70$ GPa, $\gamma = 1.75$ J/m^2 for glass [12], and average $L = 600$ nm for the coatings, we can calculate E_c to be $\approx$ 9 GPa for nanotube coatings and $\approx$ 6 GPa for clay coatings, respectively. These values are reasonably consistent with the calculated theoretical values by rule of mixture (ROM), which are 8 GPa and 3 GPa, respectively, for the two corresponding nanocomposite coatings.
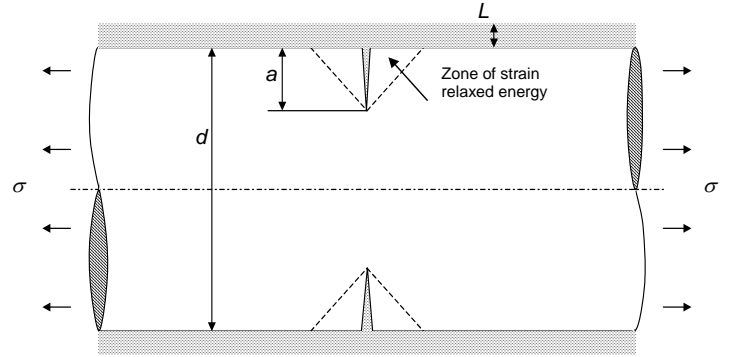

Fig. 5. A sketch of a coated fiber with a surface flaw. The fiber is loaded in tensile stress s and the circumferential surface flaw of length a serves as an initial crack. The fiber diameter and coating thickness are given by d and L, respectively, where a and L are much less than d.
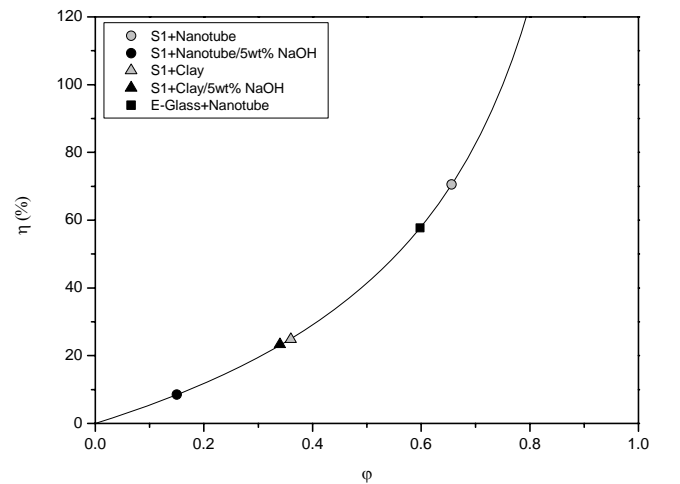

Fig. 6. Response of strength variation ratio η to healing efficiency factor φ.

3.3 Fiber bending strength

To substantiate further the role of nanocoatings in mechanical improvement, we carried out single fiber loop bending test. Fig. 7a shows an example of the shape of a ARG fiber, in which the radius of curvature at failure was measured, also shows the fracture surface of a fiber observed by the AFM phase imaging. The AFM scan shows a variety of
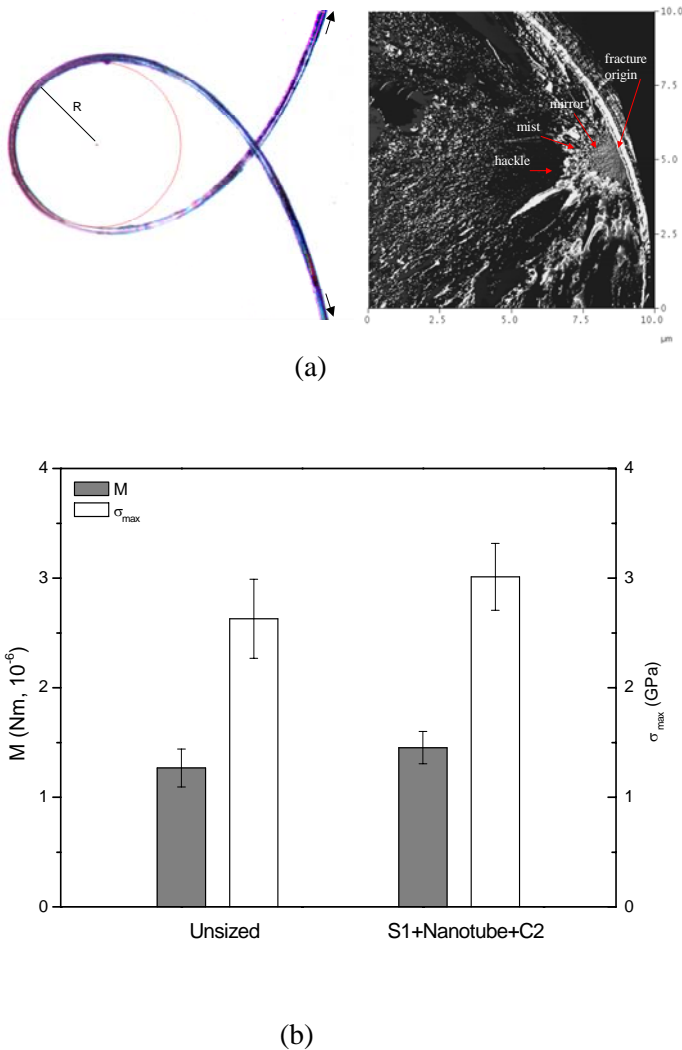

(a)

(b)

Fig. 7. Bending properties of ARG fibers: (a) shape of ARG fiber during the loop test and AFM phase image of its failure cross-section. (b) effect of the nanostructed coatings with low fraction of nano-reinforcements on the failure bending moment and maximum stress of ARG fibers. Error bars represent standard deviations for the estimate of the mean values of fifteen samples.

features of fracture phenomena from micrometer to nanometer scale, where a representative fracture mirror, mist, hackle, and branching pattern on a fracture surface can be observed. It is well known that the crack front initially produces the smooth mirror region. As the crack accelerates it becomes more unstable, creating a dimpled surface known as mist. This instability eventually causes the crack to branch out, producing the rough hackle region. The hackle region is characterized by elongated markings that proceed in the direction of crack propagation and the hackle markings point back to the flaw origin on the edges. Based on the high sensitivity of AFM phase image, we also observed the fine marks in mirror region which point back to the flaw origin in more detail. The distance from the fracture origin to the onset of the mist is referred to as the mirror radius. It would be of interest to relate the mirror radius to mist to the magnitude of the stress, σ, at failure by an empirical relation of the form: $\sigma = A \, / \, R_m^{1/2}$ [13]. R_m indicates the mirror radius which is about 1.2 mm in this sample. A is the empirically derived constant which is 2.1 MPa $\times$ m$^{1/2}$ for silica fiber [14]. Therefore, the calculated failure stress is about 1.9 GPa, which is in a fairly good agreement with above measured fiber tensile strength. The verification of the above relationship between stress and mirror radius, simply by measuring the mirror radius on a failed component, is important for quantitative fractography to estimate the failure stress with good precision over a wide range of applied stresses. In addition, it is critical to determining the location and reason which cause the failure event.

The corresponding failure bending moment and the maximum bending stress in the bending test are presented in Fig. 7b. As expected, both values of nanotube coated fibers are higher compared to those of the unsized fibers. Similar to the tensile test, the data scatter in the bending strengths decrease after surface coating, suggesting that the healed flaws on the coated fibers show similar flaw size as aforementioned. However, it is interesting to note that the effect of coating on bending properties leading to an increase of less than 20% seems not as remarkable as on the tensile properties. The most plausible explanation for this behavior is that the maximum stress subjected to tension during bending only involves a small strip of the surface region at the outside top of the loop compared to the whole fiber surface area. In addition, the gauge length of ~ 3 mm in the loop test is considerably shorter than

that of 20 mm in the tensile test. In comparison with the case of tensile tests, therefore, only a small fraction of coating, on this small strip region of the relatively short length of fiber, is in active states for efficient healing. Importantly, in view of statistics, with decreasing efficient specimen surface area to the small strip surface region, the chance of finding a large flaw decreases. According to the healing efficiency factor, φ, and Eq. 4, the bigger the surface defects the more improvement in strength could be achieved by nanocoatings. Thus, the healing effect for these sub-critical flaws in this region will be less significantly revealed in the loop test. It is also worth of mentioning that the calculated maximum stress at fiber edge is 2.6~3 GPa which is higher than the values of above tensile strength. This is because the measured strength depends on the length/volume of the test fiber. As aforementioned, the gauge length in the loop test is considerably shorter than that in the tensile test, therefore higher strength in loop test is obtained.
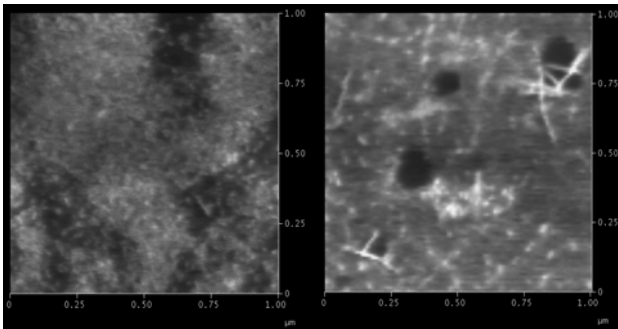
a)   b)

Fig. 8. AFM Phase images of fracture surfaces of a) E-glass fibers without SWCNTs and b) E-glass fibers with SWCNTs in sizing after fiber pull-out test (x, y =1 µm, z = 100°).

3.4 Interfacial adhesion

To investigate whether the nanocoatings could affect interfacial adhesion, we finally tested the both concrete and PP matrix composites with nanocomposite coated ARG and E-glass fibers. In comparison of the systems without clay (see Table 1), the sized fiber with clay shows a significantly higher local interfacial shear strength τ_d and critical interfacial energy release rate G_{ic}. We applied additional polymer coating with clay on the sized

fiber which shows the best performance. The significant increase in adhesion strength is attributed to the mechanical properties and thickness of the hybrid nanocoatings, influencing interface integration and stress concentration. Besides, the coating with clay results in a much less degradation due to limited access of the aggressive alkali solution, which consequently increase the frictional component of bond.

Table 1. Local interfacial shear strength, τ_d, and critical interfacial energy release rate, G_{ic}, of ARG fiber reinforced cement and PP matrix composites

Fiber/Matrix	τ_d (MPa)	G_{ic} (J/m^2)
ARG Control/Cement	23	0.6
ARG Coating C2/Cement	25	0.7
ARG S1+Clay/Cement	34	2.2
ARG S1+Coating K+Clay/Cement	57	5.7
E-glass PP sizing/PP	22	14.0
E-glass PP sizing+SWCNTs/PP	30	31.8

Our approach was further extended for single-walled carbon nanotubes (SWCNTs)/E-glass fiber reinforcements and thermoplastic polypropylene filaments using commingled yarn technologies. The in-situ commingling enables to combine homogeneously both glass and polypropylene filament arrays in one processing step and without fiber damage compared to commingling by air texturing [15]. We found that the local adhesion strength and the critical interface energy release rates are significantly improved for sizings with SWCNTs system (Table 1). Regarding the fracture surface after pull-out, it is interesting that some small coarse texture can be observed for SWCNTs system and its roughness is increased (Fig. 8), which is likely to involve mechanical interlinking (anchor effect) of carbon nanotubes against matrix

deformation/ cracking. We suggest that different nanotube related toughening mechanisms underlie the multi-scale interfacial fracture behaviour, including glass fiber/nanotube/matrix interfacial debonding, nanotube pull-out, and interfacial crack bridging. Additional data are clearly desirable and a more thorough study is required based on a fractal dimension approach to built an energy-geometry link between critical interphase energy release rate by micromechanical testing and detailed fracture surface features.

4 Conclusions

An experimental investigation of nanocomposite coatings for healing surface flaws of glass fibers and improving alkali-resistance was performed. We found that, with low fraction of nanoreinforcements, the nanostructured and functionalised traditional glass fibers show significantly improved both mechanical properties and environmental corrosion resistance. The most remarkable mechanical strength improvement is found for glass fibers with nanotube coatings, corresponding to the highest healing efficiency factor. Our study reveals that the coating modulus, thickness and roughness are responsible for the mechanical enhancement. No apparent strength variation appears for nanoclay coated fiber subjected to alkaline attack, which indicates that the influence of moisture solvent uptake and concentration on mechanical properties decreases when the organoclay is dispersed in coating polymer. Besides, nanocomposite coatings result in higher fiber/matrix interfacial adhesion, suggesting nanotube related interfacial toughening mechanisms. Overall, the hybrid nanocoatings cause improved fiber strength, corrosion resistance, and interfacial properties.

References

[1] Gao SL., Mäder E., Abdkader A. and Offermann P. "Sizings on alkali-resistant glass fibers: environmental effects on mechanical properties". *Langmuir*, Vol.19, No.6, pp 2496-2506, 2003.

[2] Gao SL., Mäder E., Plonka R. and Liu JW. "Surface flaw sensitivity of glass fibers with nanoreinforcement in polymer coating". *Proceedings of 15th Intern. Conf. Compos. Mater. (ICCM-15)*, CD-ROM, 1-10, ISBN:1-86840-589-3, Durban, South Africa; July 2005.

[3] Vigolo B., Penicaud A., Coulon C., Sauder C., Pailler R., Journet C., et al. "Macroscopic fibers and ribbons of oriented carbon nanotubes". *Science* , Vol. 290, No.5495, pp 1331–1334, 2000.

[4] Ericson LM., Fan H., Peng HQ., Davis VA., et al. "Macroscopic, neat, single-walled carbon nanotube fibers". *Science* , Vol. 305, No.5689, pp 1447–1450, 2004.

[5] Eitel W. and Oberlies F. "Einige Eigenschaften des Glasfadens". *Glastechn. Ber*, Vol.15, No.6, pp 228-231, 1937.

[6] Zhandarov S., Pisanova E. and Mäder E. ''Is there any contradiction between the stress and energy failure criteria in micromechanical tests? Part II. Crack propagation: Effect of friction on force-displacement curves''. *Compos Interface*, Vol.7, pp 149–175, 2000.

[7] Zhandarov S. and Mäder E. ''Indirect estimation of fiber/polymer bond strength and interfacial friction from maximum load values recorded in the microbond and pull-out tests. Part II: Critical energy release rate''. *J Adhes Sci Technol.*, Vol. 17, pp 967–80, 2003.

[8] Gao SL., Mäder E. and Plonka R. ''Nanostructured coatings of glass fibers: Improvement of alkali resistance and mechanical properties''. *Acta Materialia*, Vol.55, pp 1043–1052, 2007.

[9] Yano K., Usuki A., Okada A., Kurauchi T. and Kamigaito O. ''Synthesis and properties of polyimide–clay hybrid''. *J Polym Sci Part A Polym Chem* , Vol.31, pp 2493-2498, 1993.

[10] Lan T., Kaviratna PD. and Pinnavaia TJ. ''On the Nature of Polyimide-Clay Hybrid Composites''. *Chem Mater*, Vol.6, pp 573-575, 1994.

[11] Gao SL., Mäder E. and Plonka R. ''Coatings for fiber and interphase modification in a cementitious matrix''. *Acta Materialia*, Vol. 52, pp 4745-4755, 2004.

[12] Lawn BR. ''Fracture of Brittle Solids''. 2nd edition, Cambridge Univ. Press: Cambridge, 1993.

[13] Shand EB. ''Breaking stress of glass determined from dimension of fracture mirrors''. *J Amer Ceram Soc.*, Vol.42, pp 474-477, 1959.

[14] Mecholsky JJ. ''Fracture surface analysis of optical fibers''. Ceramics and Glasses of the Engineered Materials Handbook, Vol. 4, pp. 663-668, ASM International, 1991.

[15] Mäder, E., Rothe, C., Brünig, H. and Leopold, T. ''Online spinning of commingled yarns - equipment and yarn modification by tailored fiber surfaces''. *Key Eng Mater.*, Vol. 334-335, pp 229-232, 2007.